ECS Transactions, 25 (8) 23-32 (2009)
10.1149/1.3207572 ©The Electrochemical Society

Electrical Properties of Plasma-Deposited Silicon Oxide Clarified by Chemical Modeling

A.Y. Kovalgin[a], A. Boogaard[a], I. Brunets[a], A.A.I. Aarnink[a], and R.A.M. Wolters[a,b]

[a] MESA+ Institute for Nanotechnology, University of Twente, Chair of Semiconductor Components, P.O. Box 217, 7500 AE Enschede, The Netherlands
[b] NXP Research Eindhoven, HTC 4, 5656AA Eindhoven, The Netherlands.

Our study is focused on Plasma Enhanced Chemical Vapor Deposition (PECVD) of silicon dioxide films at low temperatures (< 150 ^{o}C) using Inductively Coupled (IC) High-Density (HD) plasma source. We recently fabricated Thin Film Transistors (TFTs) with high-quality ICPECVD gate oxides, which exhibited a competitive performance. For better understanding of the influence of deposition parameters on both the deposition kinetics and oxide quality, we have modeled the Ar-SiH_4-N_2O plasma system with 173 chemical reactions. We simulated concentrations of 43 reactive species (such as e.g. SiH_x radicals and SiH_x^+ (x=0-3) ions, polysilanes, SiO, SiN, SiH_3O, SiH_2O, HSiO, etc., as well as atomic hydrogen, nitrogen and oxygen) in plasma. We further used our simulations to qualitatively explain (in terms of concentrations of the reactive species) the influence of SiH_4/N_2O gas-flow ratio and total gas pressure on film electrical properties and deposition rate.

Introduction

Deposition of high-quality silicon oxide in the temperature range 50-400 ^{o}C attracts much attention for enabling e.g. CMOS post-processing and 3D device integration (1-4). We recently demonstrated TFTs with competitive mobility values, good ring oscillator performance and low off-state currents (6). This competitive TFT performance was among others enabled by the high-quality plasma-deposited SiO_2, which could be realized having sufficient understanding of the impact of plasma-deposition conditions on film (electrical) properties. Based on chemical modeling, this understanding led to optimization of process parameters.

An accurate model requires exact knowledge of plasma conditions that strongly affect plasma chemical composition. The latter determines the film composition and its (electrical) properties. Modeling using “generally-accepted” plasma characteristics (e.g. Maxwell - Boltzmann (MB) Electron Energy Distribution Function - EEDF) without their practical verification for a given plasma reactor can lead to a significant discrepancy between the actual and modeled deposition conditions (7).

In this work, we present our latest results on chemical modeling of an ICPECVD reactor intended for low-temperature (<150 ^{o}C) deposition of silicon oxide films in Ar-SiH_4-N_2O plasma. We have continued our earlier work (8) where we modeled chemical reactions in Ar-SiH_4 plasma by considering a set of 16 electron impact- and 26 secondary-homogeneous reactions. In the current work, we extended the model to Ar-SiH_4-N_2O-(H_2-N_2-O_2) plasma system with 173 reactions in total. This enabled chemical

Downloaded 29 Sep 2009 to 130.89.18.35. Redistribution subject to ECS license or copyright; see http://www.ecsdl.org/terms_use.jsp

modeling of silicon oxide and silicon nitride deposition processes in comparison with modeling of *a*-Si deposition in our earlier research.

The purpose of this work is neither to give an extended overview of the film properties nor to demonstrate the best optimized examples. The best-quality films were already briefly presented in (5). They exhibited very low leakage currents at the electric field strength of 6.5 MV/cm, comparable to the leakage currents of thermally grown oxides. A very low midgap interface state density of $3 \cdot 10^{10}$ $eV^{-1} \cdot cm^{-2}$ was obtained. These films were successfully applied in the fabrication of low-temperature TFTs with a competitive performance (6, 9).

The purpose of this work is to demonstrate that modeling of gas-phase reactions can contribute significantly to understand properties of films deposited at different deposition conditions. In this work, we show the influence of total gas pressures and initial silane fraction in plasma on deposition rate, optical and electrical thickness, leakage current and electrical charge of the films.

Deposition set-up

The experimental ICPECVD system, used for the oxide deposition, is described elsewhere (10, 11, 12). Argon (100 or 190 sccm) was used as a carrier gas, the process pressure ranged from 1 to 6 Pa, while the total flow was fixed at 244 sccm. A flow of 44 sccm of nitrous oxide (N_2O) was added to the carrier gas in the plasma zone, while 100 or 10 sccm of Ar-SiH_4 mixture (2% silane (SiH_4) in argon) was added downstream of the plasma. This resulted in an N_2O fraction of 18 volume % and in a SiH_4 fraction of 0.8 or 0.08 %, respectively.

For the experiments we used 100-mm (100)-oriented *n*-type Si wafers having a resistivity of 1-10 Ω·cm. The wafer cleaning consisted of a 10-min immersion into 100% fuming HNO_3 and a 10-min immersion into boiling 69% HNO_3, followed by a 30-s dip into 1% HF in order to remove the chemical oxide and passivate the surface. SiO_2 layers in the thickness range between 40 and 55 nm were deposited at total gas pressures 1-6 Pa and a substrate temperature of 150 °C.

Film properties

To measure the electrical properties, MOS capacitors were realized by sputtering a 1−μm thick aluminum layer onto the deposited oxide, followed by lithography and etching processes to define 0.06, 0.1 and 0.2 mm^2 capacitors. An aluminum layer of the same thickness was also sputtered on the backside of the Si wafer. All the properties were obtained for as-deposited films. The high frequency (10 kHz) capacitance-voltage (*C-V*) and current density-voltage (*J-V*) measurements were carried out using a Hewlett-Packard 4275A and a Hewlett-Packard 4140B pA meter, respectively.

The optical thickness and relative mass density of the deposited oxides were determined *in-situ* by a M2000 spectroscopic ellipsometer (SE, spectral range of 245–1700 nm), manufactured by J.A. Woollam, Inc. The SE data were analyzed by a two-layer optical model; from bottom to top: silicon, silicon oxide. The relative density was determined by a Bruggeman Effective Medium Approximation (EMA) by introducing voids.

Downloaded 29 Sep 2009 to 130.89.18.35. Redistribution subject to ECS license or copyright; see http://www.ecsdl.org/terms_use.jsp

Deposition Rate and Optical Film Thickness

Silane fraction of 0.8 %. The SiO_2 deposition rate unexpectedly decreased from 4.7 nm/min at 2 Pa to 3.5 nm/min at 6 Pa (see Table I), whereas one could practically expect a higher deposition rate at 6 Pa due to the higher concentration of electrons and initial silane at this pressure. The SE measurements additionally indicated a lower relative material density at 1-2 Pa compared to 6 Pa. The lower density could be caused by building an inappropriate chemical network resulting in nano- or micro-voids. Namely, the measured at 632 nm refractive index (n) was 1.42 at total pressures of 1 and 2 Pa, whereas at 6 Pa n increased to its normal value of 1.46 for stoichiometric SiO_2.

TABLE I. Properties of as-deposited SiO_2 Layers.

Total Pressure, Pa	SiH_4 Fraction, %	Dep. Rate, nm/min	Opt. thick., nm	Rel. Density (Therm. Ox.)	Elect. thick., nm	Flatband Voltage, V
1	0.8	4.4	50	0.97	26	-2.5
2	0.8	4.7	54	0.97	24	-1.6
6	0.8	3.5	42	0.99	40	-1.3
1	0.08	0.58	47	1.00	48	-0.74
2	0.08	0.63	50	1.00	53	0.21
6	0.08	0.62	51	0.97	28	-0.62

Silane fraction of 0.08 %. The SiO_2 deposition rate remained approximately 0.6 nm/min for the entire pressure range 1-6 Pa (see Table I). A small increase of the deposition rate at 2 and 6 Pa compared to 1 Pa still can bee seen. The measured n was in this case 1.46 at total pressures of 1 and 2 Pa, whereas at 6 Pa n decreased to 1.42. This indicated the stoichiometric Si/O ratio of the material and its appropriate density at 1-2 Pa, and a lower material density at an elevated pressure of 6 Pa, as shown in Table I.

Electrical Film Thickness

Silane fraction of 0.8 %. From the *C-V* measurements, we calculated the electrical oxide thickness by using the dielectric constant of stoichiometric SiO_2 and compared that with the optical film thickness obtained by SE. The use of the dielectric constant of SiO_2 resulted in the electrical film thickness lower than the measured optical thickness for films deposited at 1 and 2 Pa. Both the electrical and optical methods measured quite similar thicknesses for films deposited at 6 Pa.

The lower electrical thickness at 1-2 Pa could be explained by the abovementioned lower material density caused by voids. The voids led to the incorporation (adsorption) of water in the films formed at 1-2 Pa, during their exposure to air. As the electrical thickness was ~46% lower (Table I), we calculated that this accounted for approx. 2% of water in the layers. Roughly approximating, $\varepsilon_{effective} = x \cdot \varepsilon_{H2O} + (1-x) \cdot \varepsilon_{SiO2}$, where $\varepsilon_{effective}$ is the effective dielectric constant of the oxide, x is the volume fraction of water, and ε_{SiO2} (3.9) and ε_{H2O} (80) are the dielectric constants of stoichiometric silicon dioxide and water, respectively.

Silane fraction of 0.08 %. From the *C-V* measurements, we again noticed a strong influence of total pressure on the electrical oxide thickness. The effect of the pressure was, however, opposite compared to that at the higher silane fraction (see Table I). Namely, the use of the dielectric constant of SiO_2 resulted in the electrical film thickness lower than the measured optical thickness for the film deposited at 6 Pa. In contrast to

Downloaded 29 Sep 2009 to 130.89.18.35. Redistribution subject to ECS license or copyright; see http://www.ecsdl.org/terms_use.jsp

this, both the electrical and optical methods revealed similar thicknesses of films deposited at 1 and 2 Pa.

Leakage Current

The leakage currents were extracted from the corresponding *J-V* curves. The actual voltages at the semiconductor interface were corrected for the flatband voltages (V_{fb}) of the corresponding *C-V* measurements. The oxide electric fields (*E*) were calculated from the actual voltages and for the given optical film thicknesses.

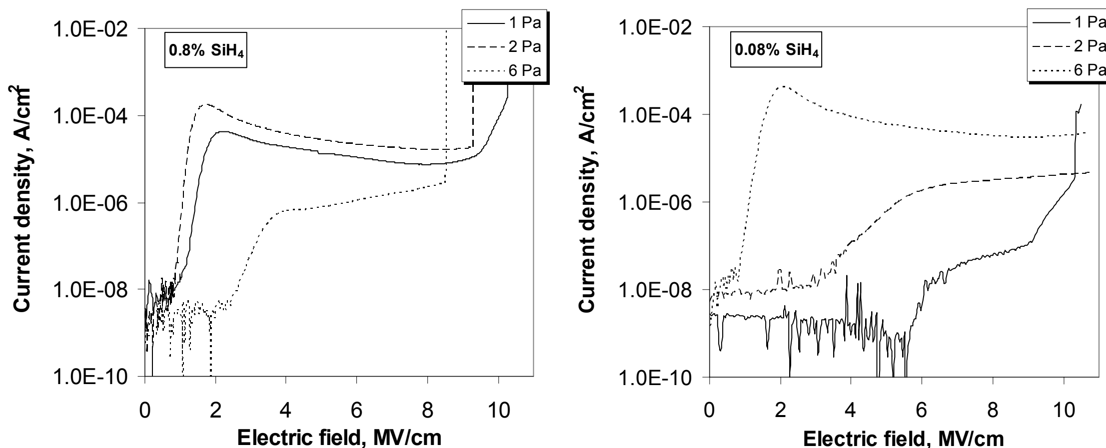

Figure 1. *J-V* characteristics of as-deposited ~50-nm thick SiO_2 layers. The electric field (*E*) is calculated as (V-V_{fb}) divided by the optical thickness. Conditions: 0.8 volume % (left) and 0.08 volume % (right) of SiH_4; total gas pressures 1-6 Pa.

Silane fraction of 0.8 %. It appears that the layers deposited at a pressure of 1 Pa exhibit a relatively high leakage current (Fig. 1, left). The current density reaches its maximum at already a low electric field of 2 MV/cm, which indicates a high concentration of traps. The ledges between 2 and 8 MV/cm, are probably related to a conduction mechanism caused by such traps. The traps can be caused, for example, by extra silicon (15). However, the measured *n* of 1.42 (1-2 Pa) rather points to the lower-density than silicon-rich films. According to (16), the concentration of extra silicon must exceed 0.7 volume % to increase *n* up to 1.47 (assuming appropriate density). In our case, the traps are more likely caused by building inappropriate chemical network (e.g., dangling Si bonds or Si-H bonds), as a result of the mentioned lower material density (see Table I). Remarkable, the leakage current decreases roughly by a factor of 100 with increasing the deposition pressure to 6 Pa (Fig. 1, left).

Silane fraction of 0.08 %. Unlike the higher SiH_4 fraction, the layers deposited at a pressure of 6 Pa exhibit a high leakage current (Fig. 1, right). The leakage current drops within approximately two orders of magnitude with decreasing the pressure to 2 Pa, and another 2 orders of magnitude when the pressure is further decreased to 1 Pa.

Oxide Electric Charge

There are two general effects to be seen in Table I. First, the V_{fb} shifts from negative to less negative values (meaning the formation of a less positive or sometimes even negative charge (5) in the films) with increasing total pressure. This effect is more pronounced for the high SiH_4 fraction. The second observation is that a higher SiH_4

Downloaded 29 Sep 2009 to 130.89.18.35. Redistribution subject to ECS license or copyright; see http://www.ecsdl.org/terms_use.jsp

fraction of 0.8% results on average in more negative V_{fb} and thus more positive oxide charge compared to the 10-times lower SiH_4 fraction.

To clarify the origin of the charge, one has to consider irregularities of the chemical network (i.e. traps) in the oxide. At least two types of traps are identified for thermally grown oxide (17). The first type is attributed to trivalent silicon (i.e. ≡Si·, also called a silicon atom with a dangling bond) and appears to be neutral before releasing an electron (or capturing a hole). These traps become positively charged after the electron release. The second type is attributed to non-bridging oxygen, i.e. ≡Si-O·. Such a non-bridging oxygen atom requires an extra electron to complete its outer electron orbital, or an extra chemical bond to become a bridging atom. It is likely that these traps can capture electrons and thus become negatively charged.

It is known that *atomic* hydrogen passivates the traps when e.g. an aluminum gate is present (18). In this light any ambient, containing H atoms, can provide the required passivation of the traps by forming the relatively stable ≡Si-H and ≡Si-OH bonds. However, an exposure to H-containing plasma can also have the opposite effect if the so-called atomic hydrogen abstraction dominates (19, 20). The latter means an interaction of the adsorbed (chemically bonded) H atom with a free H atom impinging on the surface, which results in the H_2 desorption and thus leaving an unsaturated bond i.e. a trap. A high H-density in plasma can therefore have a negative effect on the trap passivation and increase the amount of ≡Si· dangling bonds and, thus, the positive charge in the oxide.

Clarifying film properties by modeling

Our approach on modeling, used for the result clarification, is described in (7). Briefly, we used EEDFs, experimentally measured by a Langmuir probe (LP) for non-depositing Ar- and Ar-N_2O plasmas with an N_2O fraction of up to 18 volume %, at total gas pressures 1-6 Pa (10). These conditions resembled the actual deposition conditions. We further performed Optical Emission Spectroscopy (OES) measurements to examine the impact of small additions of SiH_4 on relative intensities of given emission lines of Ar and, thus, on the EEDF itself (11). We observed no significant impact of the additions of N_2O and SiH_4 to Ar plasma on the EEDF shape at the conditions studied. Contrary, the electron density (n_e) was significantly (1-2 orders of magnitude) decreased by adding N_2O (Fig. 2A). The latter was in agreement with the direct measurements of n_e by LP (7). Small additions of SiH_4 slightly increased the n_e.

To calculate the reaction rate constants for the selected electron-impact reactions in Ar-SiH_4-N_2O-(H_2-N_2-O_2) plasma system at 1-6 Pa, we used the reaction cross-sections from literature (see (7) for the reactions and references) and the EEDFs obtained by LP for pure-Ar plasmas at corresponding pressures. The corresponding n_e was corrected accordingly to the initial plasma composition and the pressure (see Fig. 2A). Combining the calculated (electron-impact reactions) and obtained from the literature (homogeneous reactions) reaction rate constants (see (7) for details), we simulated concentrations of 43 reactive species in plasma such as SiH_x radicals and SiH_x^+ (x=0-3) ions, polysilanes, SiO, SiN, SiH_3O, SiH_2O, HSiO, etc., as well as atomic hydrogen, nitrogen and oxygen.

Summarizing, the following effects are aimed to be explained by our modeling. First, for a *SiH_4 fraction of 0.8%*, we observed 1) lower SiO_2 density and more traps in the films deposited at the lowest pressure (1 Pa): this resulted in the higher leakage

Downloaded 29 Sep 2009 to 130.89.18.35. Redistribution subject to ECS license or copyright; see http://www.ecsdl.org/terms_use.jsp

current; 2) close-to-normal SiO_2 density and less traps in the films deposited at the highest pressure (6 Pa): this led to the lower leakage current; 3) contrary to the expectations, a 20 % decrease of the deposition rate at 6 Pa compared to 1 Pa; and 4) higher positive charge in the oxide compared to that for the lower SiH_4 fraction. Second, for a 10-times lower *SiH_4 fraction of 0.08%*, the effects were opposite with regard to the pressure. We namely obtained 1) close-to-normal SiO_2 density and less traps in the films deposited at the lowest pressure: this led to the lower leakage current; 2) lower SiO_2 density and more traps in the films deposited at the highest pressure: this resulted in the higher leakage current; 3) deposition rate hardly affected by the pressure, and 4) lower positive charge in the oxide compared to that for the higher SiH_4 fraction.

To explain the summarized observations, we refer to a given plasma composition. This determines in our model the deposition rate by means of considering relative plasma-densities of Si-containing radicals and their sticking probabilities. The composition will also determine the film stoichiometry and mass density, and the concentration of charge-trapping centers in the form of e.g. ≡Si· dangling bonds.

The film mass density can be influenced by sticking probabilities of dominating Si-containing radicals. It is known that SiH_3 radicals have the longest lifetime before they react at the surface. They have a smaller sticking probability (0.28 below 400 °C according to (21)) and can therefore experience several adsorption sites before reacting (22, 23). This leads to a conformal coverage and appropriate film density. In contrast, the sticking probability of Si radicals is close to unity (on an *a*-Si:H surface) even at room temperature (24, 25). As they can react on contact, they are not able to migrate over the film; their dominant flux to the surface will lead to the formation of films with less appropriate chemical network, resulting in a lower mass density (voids).

The oxide leakage current is strongly influenced by the material density and the concentration of charge-trapping centers. A lower density at the same physical thickness is caused by nano- or micro-voids and will result in a higher leakage current. This current can also be enhanced by traps. The fixed positive oxide charge is related to the concentration of charge-trapping centers. The latter can appear after ionizing for example ≡Si· dangling bonds and forming $\equiv Si^+$ ions.

The role of N_2O in forming SiO_2 is mainly to provide atomic oxygen to the plasma. Depending on the conditions, the calculated concentration of O varies between 10^{13} and 10^{15} atoms/cm^{-3}, i.e. is approximately 1-2 orders of magnitude higher than that of SiH_x (x=0-3) radicals. The fluxes of O and SiH_x species to the surface result in the heterogeneous formation of SiO_2 films. Atomic N, also produced as a result of N_2O dissociation, is however less reactive compared to O. Homogeneous reactions between OH_y (y=0-1), NH_z (z=0-2) and SiH_x species cause the appearance of SiO, HSiO, SiH_2O, SiH_3O, H_2SiNH_2, H_3SiNH, and SiN products in gas phase (26-32). These species can additionally participate in the film formation process.

Figure 2A shows the electron densities, corrected by OES for Ar-N_2O-SiH_4 plasma compared to pure-Ar plasma, used for the calculations. As mentioned, the EEDFs are less affected by the plasma composition at the conditions studied. Therefore, EEDFs of pure-Ar plasma at the corresponding pressures are considered. Figs. 2B and 3 depict the simulations results carried out for both the SiH_4 fractions in plasma. Table II summarizes the densities of important species in plasma.

Downloaded 29 Sep 2009 to 130.89.18.35. Redistribution subject to ECS license or copyright; see http://www.ecsdl.org/terms_use.jsp

A.

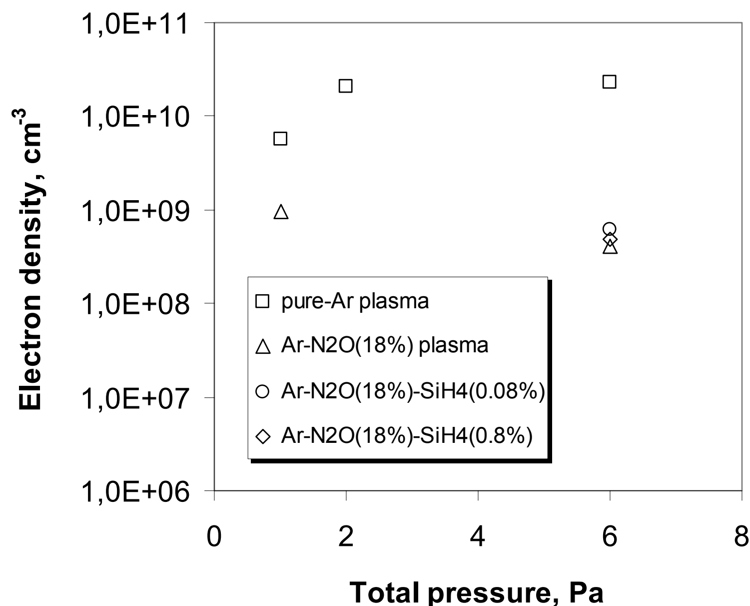

B.

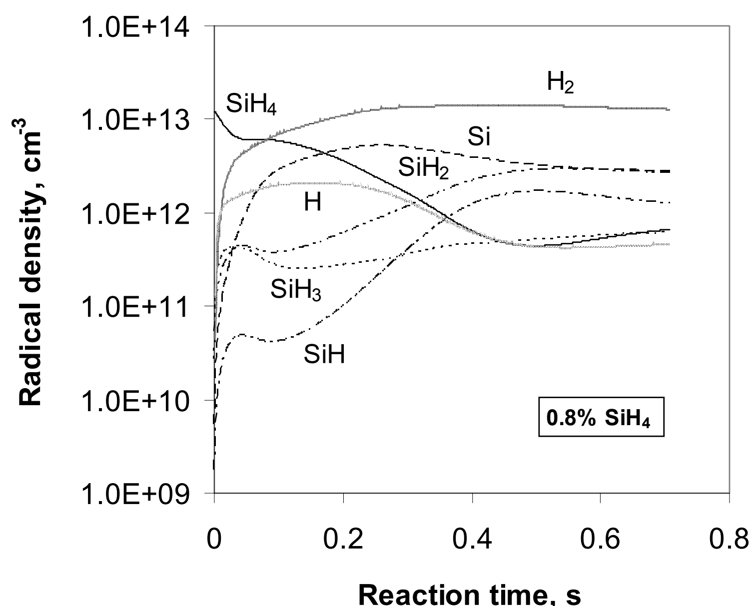

Figure 2. A – electron densities versus total pressure, experimentally measured by LP for pure-Ar plasma and corrected by OES for Ar-N_2O(18%), Ar-N_2O(18%)-SiH_4(0.08%) and Ar-N_2O(18%)-SiH_4(0.8%) plasmas. B - radical densities versus reaction time, calculated for Ar flow of 100 sccm, N_2O flow of 44 sccm, and Ar/SiH_4-mixture flow of 100 sccm (2 % of SiH_4 in Ar gives 0.8 volume % of SiH_4) at 6 Pa. See also Fig. 3.

TABLE II. Calculated Densities of Important Species in Ar-N_2O(18%)-SiH_4 plasma ($\times 10^{12}$ cm^{-3}).

Total Pressure, Pa	SiH_4 Fraction, %	O	H	H_2	Si	SiH	SiH_2	SiH_3
1	0.8	41	7.4	0.8	2.2	0.003	0.002	0.0003
6	0.8	32	0.44	14.3	3.2	1.7	2.9	0.5
1	0.08	47	0.85	0.02	0.2	0.00004	0.00002	0.00006
6	0.08	251	4.9	0.00001	1.2	-	-	-

Downloaded 29 Sep 2009 to 130.89.18.35. Redistribution subject to ECS license or copyright; see http://www.ecsdl.org/terms_use.jsp

A.

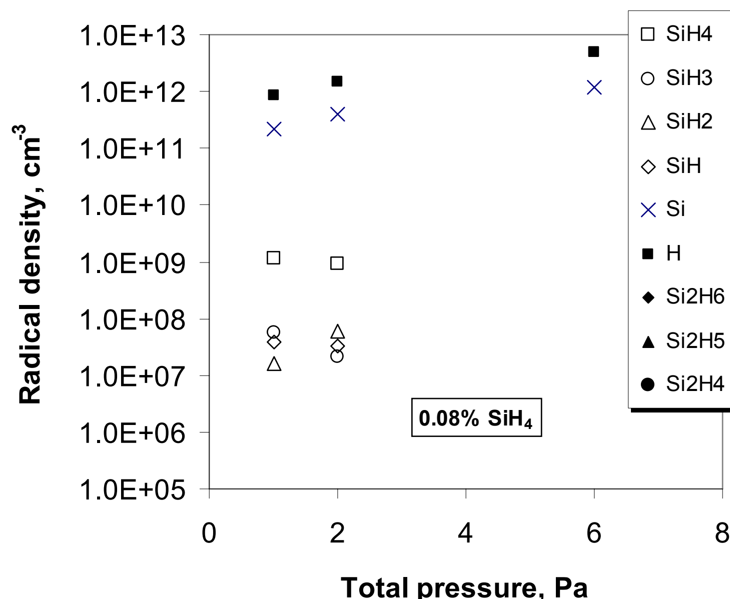

B.

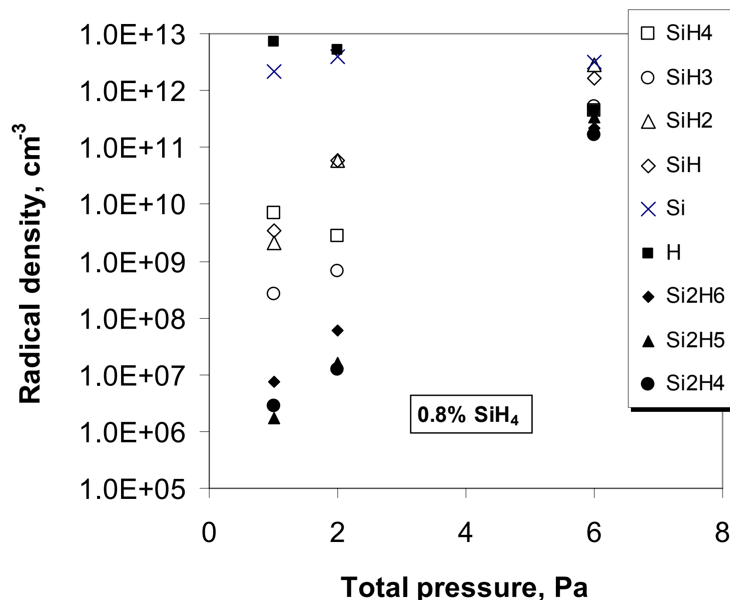

Figure 3. Radical densities, calculated based on experimental EEDFs for pure-Ar plasmas and using the n_e corrected for Ar-N_2O-SiH_4 plasmas (see Fig. 2A). Conditions - A: Ar-N_2O(18%)-SiH_4(0.08%) plasma; B: Ar-N_2O(18%)-SiH_4(0.8%) plasma.

Silane fraction of 0.8 %. Atomic silicon (sticking probability near unity) strongly dominates at 1-2 Pa (Fig. 3B). Due to the changing plasma conditions, the Si density slightly decreases at 6 Pa compared to 2 Pa. At 6 Pa, however, densities of the other SiH_x radicals increase dramatically and approach the initial level of atomic Si (see also Table II). A combination of both effects can lead to comparable deposition rates at 6 and 2 Pa.

Furthermore, because of the lower relative density of atomic Si in plasma at 6 Pa, the formation of electrically-better films is expected. This is due to a better surface migration of the other dominating SiH_x species and a lower flux of atomic Si towards the

Downloaded 29 Sep 2009 to 130.89.18.35. Redistribution subject to ECS license or copyright; see http://www.ecsdl.org/terms_use.jsp

film surface (see Table II), as discussed above. The result is that the films grow denser and therefore have lower leakage currents. The calculated density of atomic hydrogen at 6 Pa ($4.4 \cdot 10^{11}$ cm^{-3}) is significantly lower than that at 1 Pa ($7.4 \cdot 10^{12}$ cm^{-3}, see Fig. 3B and Table II). This can explain the decreased concentration of traps at 6 Pa (i.e., smaller ledges in Fig. 1, left) and less charge in the oxide (Table I). The latter effects can be caused by the diminished hydrogen abstraction at such a high pressure and therefore the inhibited formation of dangling bonds. In addition, energy of the H atoms arriving at the surface is higher at 1 Pa. This can further enhance the abstraction of hydrogen.

Silane fraction of 0.08 %. Atomic silicon dominates in plasma for the entire pressure range (see Fig. 3A and Table II). At 1-2 Pa, the other SiH_x species can still be noticed; however they disappear at 6 Pa. Deposition in the entire pressure range is in this case mainly determined by the flux of atomic Si impinging on the film. This flux gradually increases with the pressure, meaning deteriorating the film properties (see Fig. 1, right, and Table I). Still the lowest pressure of 1 Pa results in a better film quality due to the presence of small portions of the other SiH_x radicals. The calculated plasma-density of atomic hydrogen is in this case lower at 1 Pa ($8.5 \cdot 10^{11}$ cm^{-3}) compared to the density at 6 Pa ($4.9 \cdot 10^{12}$ cm^{-3}, see Fig. 3A). However, energy of the surface bombardment by H atoms is higher at 1 Pa, which can to some extent enhance the efficiency of hydrogen abstraction at this pressure. Nevertheless, the concentration of traps remains lower at 1 Pa (please compare the ledges in Fig. 1, right). Densities of atomic Si and H in plasma both increase with the pressure. We speculate that H suppresses the deposition rate at higher pressure.

Conclusions

We carried out experiments on ICPECVD of silicon dioxide films at a low temperature of 150 ^{o}C. For better understanding of the influence of SiH_4/N_2O gas-flow ratio and total gas pressure on film (electrical) properties and deposition rate, we performed chemical modeling of Ar-SiH_4-N_2O-(H_2-N_2-O_2) plasma system described by 173 chemical reactions. To explain the experimental observations, we referred to a given plasma composition and considered relative plasma-densities of Si-containing radicals and atomic hydrogen. We further explained their influence on deposition rate and mass density of the oxide, and on concentration of charge-trapping centers in the material, to clarify the measured electrical and physical film properties.

Acknowledgments

This work (project number STW 6358) is partially financially supported by the Dutch Technology Foundation (STW).

References

1. K.C. Saraswat, S.J. Souri, V. Subramanian, A.R. Joshi, and A.W. Wang, in *Proc. IEEE Int. SOI Conf.*, p. 54 (1999).
2. S. Gu, S.V. Dunton, A.J. Walker, S. Nallamothu, E.H. Chen, M. Mahajani, S.B. Herner, V.L. Eckert, S. Hu, M. Konevecki, C. Petti, S. Radigan, U. Raghuram, and M.A. Vyvoda, *J. Vac. Sci. Technol. B,* **23**, 2184 (2005).
3. N. Moussy, P. Gidon, N. Carriere, W. Rabaud, B. Giffard, B. Gluck, D. Thomas, J. Prima, F. Roy, N. Casanova, J. Regolini, J.B. Chevrier, F. Collet, A.S. Ozanne-Gomila, and O. Salasca, in *Proc. IEDM*, p. 1 (2006).

Downloaded 29 Sep 2009 to 130.89.18.35. Redistribution subject to ECS license or copyright; see http://www.ecsdl.org/terms_use.jsp

4. J. Schmitz, *Nucl. Instrum. Meth. Phys. Res. A,* **576**, 142 (2007).
5. A. Boogaard, A.Y. Kovalgin, R.A.M. Wolters, *Microelectronic Engineering*, **86**, 1707 (2009).
6. I. Brunets, A. Boogaard, S. Smits, H. de Vries, A.A.I. Aarnink, J. Holleman, A.Y. Kovalgin, and J. Schmitz, in *Proc. of the 5th Int. TFT Conference (ITC'09)*, 62 (2009).
7. A.Y. Kovalgin, A. Boogaard, R.A.M. Wolters, *Impact of Small Deviations in EEDF on Silane-based Plasma Chemistry*, accepted for *ECS Trans*., **25** (2009).
8. A.Y. Kovalgin, A. Boogaard, I. Brunets, J. Holleman, J. Schmitz, *Surface & Coatings Technology*, **201**, 8849 (2007).
9. I. Brunets, J. Holleman, A.Y. Kovalgin, A. Boogaard, J. Schmitz, *IEEE Transactions on Electron Devices,* doi:10.1109/TED.2009.2023021.
10. A. Boogaard, A.Y. Kovalgin, A.A.I. Aarnink , J. Holleman , R.A.M. Wolters, I. Brunets, and J. Schmitz, *ECS Transactions*, **2**, 181 (2007).
11. A. Boogaard, A.Y. Kovalgin, A.A.I. Aarnink , R.A.M. Wolters, J. Holleman, I. Brunets, and J. Schmitz, *ECS Transactions*, **6**, 259 (2007).
12. A. Boogaard, A.Y. Kovalgin, I. Brunets, A.A.I. Aarnink, J. Holleman, R.A.M. Wolters, J. Schmitz, *Surface & Coatings Technology*, **201**, 8976 (2007).
13. A. Hasper, J. E. J. Schmitz, J. Holleman, and J. F. Verwey, *Journal of Vacuum Science & Technology a-Vacuum Surfaces and Films*, **10**, 3193 (1992).
14. A. M. van Graven and R. A. M. Wolters, *Microelectronic Engineering*, **50**, 495 (2000).
15. D. J. DiMaria, R. Ghez and D. W. Dong, *J. Appl. Phys.*, **51**, 4830 (1980).
16. Calculated (Bruggeman EMA approximation) using CompleteEASE code, version 3.60 by J.A. Woollam Co., Inc.
17. A. R. Stivers and C. T. Sah, *J. Appl. Phys.,* **51**, 6292 (1980).
18. P. Balk, *Microelectronic Engineering*, **48**, 3 (1999).
19. K. Sinniah, M. G. Sherman, L. B. Lewis, W. H. Weinberg, J. T. Yates, Jr., and K. C. Janda, *J. Chem. Phys.* **92**, 5700 (1990).
20. D. D. Koleske and S. M. Gates, *J. Chem. Phys.* **101**, 3301 (1994).
21. J. Perrin, M. Shiratani, P. Kae-Nune, H. Videlot, J. Jolly, and J. Guillon, *J. Vac. Sci. Technol. A*, **16**, 278 (1998).
22. J. Robertson, *J. Appl. Phys.*, **87**, 2608 (2000).
23. R. Dewarrat and J. Robertson, *J. Non-Cryst. Solids*, **299-302**, 48 (2002).
24. P. Ho, W.G. Breiland, and R.J. Buss, *J. Chem. Phys.*, **91**, 2627 (1989).
25. M.D. Allendorf and R.J. Kee, *J. Electrochem. Soc.*, **138**, 841 (1991).
26. G.R.A. Johnson, *Radiation Chemistry of Nitrous Oxide Gas*, NSRDS-NBS 45 (1973).
27. K. Tokuhashi, S. Horiguchi, Y. Urano, M. Iwasaka, H. Ohtani, and S. Kondo, *Combust. Flame*, **82**, 40 (1990).
28. J.O. Chu, D.B. Beach, and J.M. Jasinski, *Chem. Phys. Lett.*, **143**, 135 (1988).
29. R. Becerra, H.M. Frey, B.P. Mason, and R. Walsh, *Chem. Phys. Lett.*, **185**, 415 (1991).
30. M. Nemoto, A. Suzuki, H. Nakamura, K. Shibuya, and K. Obo, *Chem. Phys. Lett.*, **162**, 467 (1989).
31. A. Tezaki, K. Morite, A. Miyoshi, T. Sakurai, and H. Matsui, *J. Phys. Chem.*, **99**, 1466 (1995).
32. J. Aubreton, D. Conte, J.L. Jauberteau, and I. Jauberteau, *J. Phys. D: Appl. Phys.*, **33**, 1499 (2000).

Downloaded 29 Sep 2009 to 130.89.18.35. Redistribution subject to ECS license or copyright; see http://www.ecsdl.org/terms_use.jsp